# POLITECNICO DI TORINO
# Repository ISTITUZIONALE

## Towards effective flow simulations in realistic Discrete Fracture Networks

(Article begins on next page)

04 August 2020

# Towards effective flow simulations in realistic Discrete Fracture Networks

Stefano Berrone[a], Sandra Pieraccini[a,*], Stefano Scialò[a]

[a]*Dipartimento di Scienze Matematiche, Politecnico di Torino, Corso Duca degli Abruzzi 24, 10129 Torino, Italy.*

## Abstract

We focus on the simulation of underground flow in fractured media, modeled by means of Discrete Fracture Networks. Focusing on a new recent numerical approach proposed by the authors for tackling the problem avoiding mesh generation problems, we further improve the new family of methods making a step further towards effective simulations of large, multi-scale, heterogeneous networks. Namely, we tackle the imposition of Dirichlet boundary conditions in weak form, in such a way that geometrical complexity of the DFN is not an issue; we effectively solve DFN problems with fracture transmissivities spanning many orders of magnitude and approaching zero; furthermore, we address several numerical issues for improving the numerical solution also in quite challenging networks.

*Keywords:* Fracture flows, Darcy flows, discrete fracture networks, optimization methods for elliptic problems, uncoupled large scale simulations, XFEM
*2010 MSC:* 65N30, 65N50, 68U20, 86-08

## 1. Introduction

The simulation of underground fluid flow in fractured media is a challenging issue, relevant in several critical applications, such as oil/gas recovery, gas storage, pollutant percolation, water resources monitoring. The phenomenon has a heterogeneous multi-scale nature that involves complex geological configurations. A possible approach for modelling the phenomenon is given by

---

*Corresponding author
Email addresses:* `stefano.berrone@polito.it` (Stefano Berrone), `sandra.pieraccini@polito.it` (Sandra Pieraccini ), `stefano.scialo@polito.it` (Stefano Scialò)

Discrete Fracture Networks (DFNs) [1, 2, 3, 4, 5, 6, 7, 8, 9], which are complex sets of polygonal intersecting fractures. We focus on the resolution of the steady-state flow in large fracture networks. The quantity of interest is the hydraulic head in the whole network, which is the sum of pressure and elevation, and is evaluated by means of the Darcy law. The rock matrix surrounding fractures is considered impervious such that fluid flow only occurs through fractures and fracture intersections (called traces). Hydraulic head continuity and flux balance at fracture intersections is preserved adding specific matching conditions.

Geological fractured media are characterized by a challenging geometrical complexity. A crucial issue in DFN flow simulations is the need to provide on each fracture a good quality mesh [10, 11, 12, 13]. Namely, if the meshes on the fractures are required to be conforming with the traces, and with the meshes on the intersecting fractures, the meshing process for each fracture is not independent of the process on the other fractures, thus yielding in practice a quite demanding computational effort for the mesh generation. In some cases, the meshing process may even result infeasible [10].

In [14, 15, 16] the authors proposed a PDE-constrained optimization approach for overcoming mesh generation problems related to geometrical complexities. The method has proven to be an effective numerical approach for flow simulations in DFNs. Within this approach, the exact fulfillment of hydraulic head continuity and flux balance at fracture intersections is replaced by the minimization of a cost functional, constrained by the Darcy law on the fractures. The optimization formulation, tackled with an iterative resolution method, allows for an independent meshing process and an independent resolution of the constraint equations on the fractures, thus avoiding the resolution of a huge global linear system. Various finite element based discretization techniques, such as standard FEM, XFEM or VEM have been successfully used in order to fully exploit the advantages of the method [16, 17]. The resulting method is also well suited for parallel implementation [18]. Advanced uncertainty quantification techniques have been successfully employed in conjunction with the proposed approach in [19] in order to predict the response of the method to the randomness of input data.

Here, we focus on the XFEM based discretization. In the present paper we propose a new formulation of the objective functional, aiming at improving the method towards an increased flexibility. This reformulation tackles the imposition of Dirichlet boundary conditions in weak form by means of a unified treatment of matching conditions at traces and boundary conditions at the Dirichlet boundary. In this way, the solution process does not require any knowledge concerning the reciprocal position of the traces and of the Dirichlet boundary, thus reducing the cost of the geometrical processing of

2

the network. This approach can also be useful to enforce Dirichlet boundary conditions for modeling wells or boreholes. Furthermore, when using an XFEM based discretization, the imposition of boundary conditions requires special care when traces impact or lie very close to the Dirichlet boundaries: indeed, the additional basis functions of the XFEM give a non-zero contribution on the boundary, and it might be very difficult to impose boundary conditions without affecting the behavior of the approximate solution inside the domain, [20, 21]. Furthermore, if non-smooth Dirichlet boundary conditions are to be imposed, the value of the coefficient of the XFEM additional basis functions on the Dirichlet boundary is not known in general, requiring the resolution of additional tailored local problems.

In the present work we also suggest resolution strategies in order to deal with networks of fractures characterized by a strong variability in fracture transmissivities, and/or by the presence of fractures with an hydraulic transmissivity several orders of magnitudes smaller than the others. In these situations it is beneficial to introduce some penalty terms in the functional to force an increased accuracy in the flux balance requirement. A different technique is also investigated, consisting in solving a modified problem featuring the same solution in terms of hydraulic head but with re-scaled fluxes. Finally, a preconditioner for the resolution of the discrete linear system of equations is proposed and investigated. The structure of this preconditioner is simple and effective, moreover it can be easily used for the resolution of the problem within a parallel approach.

The structure of the paper is as follows. In Section 2 the model is briefly recalled and enriched in order to introduce the weak imposition of Dirichlet boundary conditions; in Section 3 the discrete version of the problem is derived; in Section 4 we address some numerical issues mainly aimed at improving the quality of the computed solution. Finally, in Section 5 we propose some numerical results both on simple test problems and on complex and realistic DFNs in order to assess the reliability of the approach.

## 2. The continuous model

Let $\Omega$ be a DFN given by the union of open polygons $F_i$, $i = 1, \ldots, I$, resembling underground fractures. The set $\Omega$ is assumed to be connected. The intersections between fractures are called traces, and are denoted by $S_m$, $m = 1, \ldots, M$. We assume that each trace is the intersection between exactly two distinct fractures, $F_i$ and $F_j$, such that $S_m = \bar{F}_i \cap \bar{F}_j$, and we define, for further reference, the index set $I_{S_m} := \{i, j\}$. Furthermore, $\mathcal{S}_i$ denotes the set of traces on fracture $F_i$ and $\mathcal{S}$ the set of all the traces in the DFN.

3

The DFN $\Omega$ is assumed to be surrounded by an impervious rock matrix, such that the fluid flow can only occur through the fractures and across the traces. The boundary of $\Omega$, $\partial\Omega$, is divided in a Dirichlet part $\Gamma^D$ and a Neumann part $\Gamma^N$, such that $\Gamma^D \cap \Gamma^N = \emptyset$ and $\Gamma^D \cup \Gamma^N = \partial\Omega$. Similarly, the boundary of each fracture $F_i$, $\partial F_i$, is also split in a Dirichlet part $\Gamma_i^D := \partial F_i \cap \Gamma^D$ and a Neumann part $\Gamma_i^N := \partial F_i \cap \Gamma^N$. Functions $G^D$ and $G^N$ prescribe the Dirichlet and Neumann boundary conditions, whereas their restrictions to $\partial F_i$ are denoted by $G_i^D$ and $G_i^N$, respectively.

We remark that it may occur that traces are generated by the intersection of two fractures along the Dirichlet boundary, i.e., it may happen that a trace $S_m$ is a subset of the Dirichlet boundary of either one or both fractures. In both these cases we will refer to such traces as *Dirichlet traces*, whereas if $S_m \cap \Gamma_i^D = \emptyset$ for all $i = 1, \ldots, I$, we will refer to $S_m$ as an *internal trace*. In the case of a Dirichlet trace $S_m = \bar{F}_i \cap \bar{F}_j$ with, say, fracture $F_j$ intersecting $F_i$ along the Dirichlet boundary $\Gamma_i^D$, we let $F_j$ inherit, along $S_m$, the Dirichlet boundary conditions imposed on $\Gamma_i^D \cap S_m$. For the sake of uniform treatment of terms involving Dirichlet conditions, also the portions of $\Gamma_i^D$ which do not contain traces will be interpreted and treated as Dirichlet traces. Accordingly, we split the set $\mathcal{S}_i$ into two subsets $\mathcal{S}_i^D$ and $\mathcal{S}_i^{\mathrm{int}}$ containing the Dirichlet traces and the internal traces, respectively. Similarly, we split the index set $\mathcal{M} := \{1, \ldots, M\}$ into two subsets $\mathcal{M}^D$ and $\mathcal{M}^{\mathrm{int}}$ corresponding to Dirichlet and internal traces, respectively. We assume that $\mathcal{M}^D \neq \emptyset$ and $\mathcal{S}_i^{\mathrm{int}} \neq \emptyset$, for all $i = 1, \ldots, I$.

The DFN problem consists in evaluating the distribution of the hydraulic head $H$ in the network of fractures, imposing appropriate matching conditions at fracture intersections. A typical choice consists in imposing hydraulic head continuity and flux balance across the traces, and solving the Darcy equation on the fractures. This approach leads to the following classical statement of the DFN problem. Let us set $V_i^D = \mathrm{H}_{\mathrm{D}}^1(F_i) = \left\{ v \in \mathrm{H}^1(F_i) : v_{|\Gamma_i^D} = G_i^D \right\}$ and $V_i = \mathrm{H}_{0,\mathrm{D}}^1(F_i) = \left\{ v \in \mathrm{H}^1(F_i) : v_{|\Gamma_i^D} = 0 \right\}$, and let us denote by $H_i$ the restriction of $H$ to $F_i$. Then the hydraulic head in $\Omega$ is given by the following coupled system of partial differential equations: find $H_i \in V_i^D$ such that for all $v \in V_i$

$$
\begin{aligned}
\int_{F_i} \mathbf{K}_i \nabla H_i \nabla v \, \mathrm{d}\Omega \;\; &= \int_{F_i} q_i v \, \mathrm{d}\Omega + \left\langle G_i^N, v_{|\Gamma_i^N} \right\rangle_{\mathrm{H}^{-\frac{1}{2}}(\Gamma_i^N), \mathrm{H}^{\frac{1}{2}}(\Gamma_i^N)} \\
&+ \sum_{S \in \mathcal{S}_i} \left\langle \left[\!\!\left[ \frac{\partial H_i}{\partial \hat{\nu}_S^i} \right]\!\!\right]_S, v_{|S} \right\rangle_{\mathrm{H}^{-\frac{1}{2}}(S), \mathrm{H}^{\frac{1}{2}}(S)},
\end{aligned}
\tag{1}
$$

and, for $i, j \in I_{S_m}$, $\forall S_m \in \mathcal{S}_i^{\text{int}}$

$$H_{i|S_m} - H_{j|S_m} \;=\; 0, \tag{2}$$

$$\left[\!\left[\frac{\partial H_i}{\partial \hat{\nu}_{S_m}^i}\right]\!\right]_{S_m} + \left[\!\left[\frac{\partial H_j}{\partial \hat{\nu}_{S_m}^j}\right]\!\right]_{S_m} \;=\; 0, \tag{3}$$

where $\mathbf{K}_i$ is the fracture transmissivity tensor and $q_i \in \mathrm{L}^2(F_i)$ is a source term, and $\left[\!\left[\frac{\partial H_i}{\partial \hat{\nu}_{S_m}^i}\right]\!\right]_{S_m}$ represents the jump of the co-normal derivative of $H_i$ along a fixed normal direction to $S_m$.

An alternative approach is proposed in [14, 16], where the previous system of equations is replaced by a constrained optimization problem. A properly defined functional $J$ measures the lack of continuity of the hydraulic head across the traces and the lack of flux conservation across intersecting fractures. The functional is minimized subject to constraints given by the state equations. In the present work we introduce a modification of such functional, in which additional terms are introduced in order to account for a weak imposition of the Dirichlet boundary conditions.

Let us introduce, for each fracture $F_i$ and for each internal trace $S_m \in \mathcal{S}_i$ the quantity

$$U_i^m = \left[\!\left[\frac{\partial H_i}{\partial \hat{\nu}_{S_m}^i}\right]\!\right]_{S_m} + \alpha_m H_{i|S_m}, \;\; \alpha_m > 0, \; m \in \mathcal{M}^{\text{int}} \tag{4}$$

whereas for Dirichlet traces we introduce

$$U_i^m = \frac{\partial H_i}{\partial \hat{\nu}_{S_m}^i} + \alpha_m H_{i|S_m}, \;\; \alpha_m \geq 0, \; m \in \mathcal{M}^{\mathrm{D}} \tag{5}$$

and let us set

$$
\begin{aligned}
J(H, U) := \frac{1}{2} \sum_{i=1}^{I} \sum_{S_m \in \mathcal{S}_i^D} & \left( \mathcal{W}_H^D \left\| H_{i|S_m} - G_{i|S_m}^D \right\|_{\mathrm{H}^{\frac{1}{2}}(S_m)}^2 \right. \\
& + \mathcal{W}_U^D \left\| U_i^m - \frac{\partial H_i}{\partial \hat{\nu}_{S_m}^i} - \alpha_m H_{i|S_m} \right\|_{\mathrm{H}^{-\frac{1}{2}}(S_m)}^2 \bigg) \\
& + \frac{1}{2} \sum_{i=1}^{I} \sum_{S_m \in \mathcal{S}_i^{\text{int}}} \left( \mathcal{W}_H \left\| H_{i|S_m} - H_{j|S_m} \right\|_{\mathrm{H}^{\frac{1}{2}}(S_m)}^2 \right. \\
& + \mathcal{W}_U \left\| U_i^m + U_j^m - \alpha_m \left( H_{i|S_m} + H_{j|S_m} \right) \right\|_{\mathrm{H}^{-\frac{1}{2}}(S_m)}^2 \bigg) \tag{6}
\end{aligned}
$$

5

where we recall that $i, j, m$ are such that $\{i, j\} = I_{S_m}$. The quadratic functional $J(H, U)$ in equation (6) still measures the lack of continuity of the hydraulic head across the traces and the lack of flux conservation across intersecting fractures (first and second terms of the sum over the internal traces, respectively), and also accounts for a weak imposition of the Dirichlet boundary conditions (the sum over the Dirichlet traces).

In (6), $\mathcal{W}_H$, $\mathcal{W}_U$ and $\mathcal{W}_H^D$, $\mathcal{W}_U^D$ are given (possibly different) positive weights, which serve the purpose of allowing to put a larger emphasis on some terms w.r.t. the others. Indeed, the weights $\mathcal{W}_H$, $\mathcal{W}_U$ are related to the hydraulic head continuity term and flux conservation term of the functional, respectively, and $\mathcal{W}_H^D$, $\mathcal{W}_U^D$ refers to the boundary condition terms. We also note that since $\Gamma_i^D$ is allowed to be empty for some $i$ (see [16]), the first sum in $J(H, U)$ actually extends over a subset of the total number of fractures in the DFN.

**Remark 1.** *Due to (5), the term* $\left\| U_i^m - \frac{\partial H_i}{\partial \hat{\nu}_{S_m}^i} - \alpha_m H_{i|S_m} \right\|^2$ *in (6) is trivially zero, however it is introduced in order to provide a uniform treatment for both boundary and internal traces. Indeed, the corresponding weight $\mathcal{W}_U^D$ can actually be a non-negative value. Furthermore, this residual term will be not nil, in general, in the discrete counterpart of (6).*

The constraint equations (1), representing the weak formulation of the Darcy law on the fractures, are rewritten as: $\forall v \in V_i, \ \forall i = 1, \ldots, I$

$$
\int_{F_i} \mathbf{K}_i \nabla H_i \nabla v \, \mathrm{d}\Omega + \sum_{m=1}^{M} \alpha_m \int_{S_m} H_{i|S_m} v_{|S_m} \mathrm{d}\gamma =
$$
$$
\int_{F_i} q_i v \, \mathrm{d}\Omega + \left\langle G_i^N, v_{|\Gamma_i^N} \right\rangle_{\mathrm{H}^{-\frac{1}{2}}(\Gamma_i^N), \mathrm{H}^{\frac{1}{2}}(\Gamma_i^N)}
$$
$$
+ \sum_{m=1}^{M} \left\langle U_i^m, v_{|S_m} \right\rangle_{\mathrm{H}^{-\frac{1}{2}}(S_m), \mathrm{H}^{\frac{1}{2}}(S_m)}. \tag{7}
$$

As a whole, functions $U_i^m \in \mathrm{H}^{-\frac{1}{2}}(S_m)$ act as control variables for the following constrained minimization problem:

$$
\min J(H, U) \tag{8}
$$
$$
\text{subject to (7).}
$$

Being $\alpha_m > 0$ for $m \in \mathcal{M}^{\mathrm{int}}$, well-posedness of the problems on the fractures is guaranteed. The equivalence of the present formulation with the formulation (1)-(3) is straightforward, observing that the new formulation corresponds to the weak imposition of the Dirichlet boundary conditions.

## 3. The discrete problem

In the previous Section we have depicted the PDE-constrained optimization reformulation of the DFN flow problem. Here we give some details about the discrete version of problem (8). In the following, we will use lower case letters for the finite dimensional approximations of functions $H$ and $U$. Since the method here proposed is a generalization of the methods described in previous works, the following description is closely related to similar issues described by [17]. We refer the reader to such reference for further details. Without loosing generality, for the ease of description, we will set $\alpha_m = 0$ for all $m \in \mathcal{M}^D$, and $\alpha_m = \alpha$ for all $m \in \mathcal{M}^{\text{int}}$.

Let us consider a finite dimensional ($N_i$-dimensional) approximation for $V_i$, $i = 1, \ldots, I$, with a total number $N^F = \sum_{i=1}^{I} N_i$ of DOFs on the fractures. Furthermore, we number the control variable on the traces as follows. Let $S_m$ be a given internal trace, with $I_{S_m} = \{i, j\}$; assuming $i < j$, the control variables related to $S_m$ and corresponding to fractures $F_i$ and $F_j$ are denoted by $u_m^-$ and by $u_m^+$, respectively. Overloading the notation, we will use the same symbol also for the corresponding vector of DOFs. The same notation overload will apply for the hydraulic head.

Let us introduce on the spaces of the control functions $u_m^-$ and $u_m^+$ the basis functions $\psi_{m,k}^-$, $k = 1, ..., N_m^-$ and $\psi_{m,k}^+$, $k = 1, ..., N_m^+$, respectively, so that we have, for $m \in \mathcal{M}^{\text{int}}$, and for $\star = -, +$, $u_m^\star = \sum_{k=1}^{N_m^\star} u_{m,k}^\star \psi_{m,k}^\star$. As far as Dirichlet traces are concerned, let us write, for $m \in \mathcal{M}^D$,

$$u_m^D = \sum_{k=1}^{N_m^D} u_{m,k} \psi_{m,k}$$

being $\psi_{m,k}$, $k = 1, \ldots, N_m^D$, a basis for the space of the control variable $u_m^D$.

Setting $N^T = \sum_{m \in \mathcal{M}^{\text{int}}} (N_m^- + N_m^+) + \sum_{m \in \mathcal{M}^D} N_m^D$, we define $u \in \mathbb{R}^{N^T}$ concatenating vectors $u_m^-, u_m^+$ for all $m \in \mathcal{M}^{\text{int}}$ and $u_m^D$ for $m \in \mathcal{M}^D$. Furthermore, we define $h \in \mathbb{R}^{N^F}$ concatenating $h_i$, $i = 1, \ldots, I$.

A discrete counterpart of the functional $J$ defined by (6) is obtained. In order to simplify the notation, within this section we set to one the weights parameters introduced in (6); the extension to arbitrary values is straightforward. Nevertheless, non unitary weights are used for some numerical experiments proposed in Section 5. Let us consider $L^2$ norms instead of $H^{-\frac{1}{2}}$ and $H^{\frac{1}{2}}$ norms on the traces and on the Dirichlet boundary. Let us define for all $S_m \in \mathcal{S}$, for $p, q \in I_{S_m}$ (possibly $p = q$), the matrices

$$(C_{p,q}^{S_m})_{k,\ell} = \int_{S_m} \varphi_{p,k|S_m} \varphi_{q,\ell|S_m} \, d\gamma, \qquad C_{p,q} = \sum_{S_m \in \mathcal{S}_p} C_{p,q}^{S_m}. \qquad (9)$$

With a similar definition we introduce, for each fracture $F_i$, the matrix $C_{i,i}^{\Gamma_i^D} \in \mathbb{R}^{N_i \times N_i}$ as

$$(C_{i,i}^{\Gamma_i^D})_{k,\ell} = \int_{\Gamma_i^D} \varphi_{i,k|_{\Gamma_i^D}} \varphi_{i,\ell|_{\Gamma_i^D}} \, \mathrm{d}\gamma, \tag{10}$$

with the convention that if $\Gamma_i^D = \emptyset$ for some $i$, then $C_{i,i}^{\Gamma_i^D}$ is the null matrix.

Furthermore, for $m \in \mathcal{M}^{\mathrm{int}}$ and $\star = -, +$ define $\mathcal{C}_m^\star \in \mathbb{R}^{N_m^\star \times N_m^\star}$, $\mathcal{C}_m^\pm \in \mathbb{R}^{N_m^- \times N_m^+}$ and $\mathcal{C}_m$ as:

$$(\mathcal{C}_m^\star)_{k\ell} = \int_{S_m} \psi_{m,k}^\star \psi_{m,\ell}^\star \, \mathrm{d}\gamma, \quad (\mathcal{C}_m^\pm)_{k\ell} = \int_{S_m} \psi_{m,k}^- \psi_{m,\ell}^+ \, \mathrm{d}\gamma,$$

$$\mathcal{C}_m = \begin{pmatrix} \mathcal{C}_m^- & \mathcal{C}_m^\pm \\ (\mathcal{C}_m^\pm)^T & \mathcal{C}_m^+ \end{pmatrix},$$

and $B_{i,m}^\star \in \mathbb{R}^{N_i \times N_m^\star}$ as

$$(B_{i,m}^\star)_{k\ell} = \int_{S_m} \psi_{m,k}^\star \varphi_{i,\ell|_{S_m}} \, \mathrm{d}\gamma,$$

and set

$$B_{i,m} = (B_{i,m}^- \; B_{i,m}^+) \in \mathbb{R}^{N_i \times (N_m^- + N_m^+)}, \qquad u_m = (u_m^-, u_m^+).$$

For each fixed $i = 1, ..., I$, matrices $B_{i,m}$, for $m$ such that $S_m \in \mathcal{S}_i$, are then grouped row-wise to form the matrix $B_i \in \mathbb{R}^{N_i \times N_{\mathcal{S}_i}}$, with $N_{\mathcal{S}_i} = \sum_{S_m \in \mathcal{S}_i} (N_m^- + N_m^+)$. Matrix $B_i$ acts on a column vector $u_i$ obtained extracting blocks $u_m$, for $S_m \in \mathcal{S}_i$, from $u$ and appending them in the same order used for $B_{i,m}$, as the action of a suitable operator $R_i : \mathbb{R}^{N^T} \mapsto \mathbb{R}^{N_{\mathcal{S}_i}}$ such that $u_i = R_i u$. Finally, let $B \in \mathbb{R}^{N^F \times N^T}$ be defined by

$$B = \begin{pmatrix} B_1 R_1 \\ \vdots \\ B_I R_I \end{pmatrix}.$$

The matrix $\mathcal{C}_m^D \in \mathbb{R}^{N_m^D \times N_m^D}$ is defined similarly to $\mathcal{C}_m^\star$ as

$$(\mathcal{C}_m^D)_{k\ell} = \int_{S_m} \psi_{m,k} \psi_{m,\ell} \, \mathrm{d}\gamma$$

for $m \in \mathcal{M}^{\mathrm{D}}$.

Let now $G^h \in \mathbb{R}^{N^F \times N^F}$ be defined blockwise as follows: for $i = 1, ..., I$ we set

$$G_{ii}^h = (1 + \alpha^2) C_{i,i} + C_{i,i}^{\Gamma_i^D},$$

$$G_{ij}^h = (\alpha^2 - 1)C_{i,j}^S \text{ if } j \in J_i \text{ (0 elsewhere)} ,$$

where, fixed $F_i$, $J_i$ collects the indices $j$ such that $|\bar{F}_j \cap \bar{F}_i| > 0$. Note that $G^h$ is a symmetric matrix. Next, let us define the matrix $G^u \in \mathbb{R}^{N^T \times N^T}$ blockwise as

$$G^u = \begin{pmatrix} \mathrm{diag}(\mathcal{C}_m, m \in \mathcal{M}^{\mathrm{int}}) & O \\ O & \mathrm{diag}(\mathcal{C}_m^D, m \in \mathcal{M}^D) \end{pmatrix} .$$

Finally, letting $n$ be the outward normal to $\Gamma_i^D$, let us define for $i = 1, \ldots, I$ the matrices

$$(D_i)_{k\ell} = \int_{\Gamma_i^D} n^T(\mathbf{K}_i \nabla \phi_{i,k}) n^T(\mathbf{K}_i \nabla \phi_{i,\ell}) \, \mathrm{d}\gamma,$$

and

$$(D_i^u)_{k\ell} = \int_{S_m} n^T(\mathbf{K}_i \nabla \phi_{i,\ell}) \psi_{m,k} \, \mathrm{d}\gamma,$$

with $S_m \in \mathcal{S}_i^D$. Then we set

$$D = \mathrm{diag}(D_i, i = 1, \ldots, I),$$

and

$$D^u = \begin{pmatrix} D_1^u R_1' \\ \vdots \\ D_I^u R_I' \end{pmatrix} .$$

where for $i = 1, \ldots, I$ the operator $R_i' : \mathbb{R}^{N^T} \mapsto \mathbb{R}^{N_{\mathcal{S}_i}^i + N_i^D}$, with $N_i^D = \sum_{S_m \in \mathcal{S}_i^D} N_m^D$, extracts from $u$ a sub-vector containing the control variables $u_m^\star$ and $u_m^D$ which refers to traces $S_m$ on $F_i$.

The discrete functional can finally be written as

$$\begin{aligned} J &= \frac{1}{2} \left( h^T(G^h + D)h - \alpha h^T B u - \alpha u^T B^T h + u^T G^u u \right) \\ &\quad - \left( h^T h_D + h^T D^u u \right) + c \end{aligned}$$

where $h_D$ is a vector accounting for the Dirichlet data and the constant term $c$ is the sum of the square $\mathrm{L}^2$ norm of the Dirichlet boundary conditions $G_i^D$, $i = 1, \ldots, I$.

The algebraic counterpart of constraints (7) is written as follows. For all $i = 1, ..., I$ define the matrix $A_i \in \mathbb{R}^{N_i \times N_i}$ as

$$(A_i)_{k\ell} = \int_{F_i} \mathbf{K}_i \nabla \phi_{i,k} \nabla \phi_{i,\ell} \, \mathrm{d}F_i + \alpha \sum_{S \in \mathcal{S}_i} \int_S \phi_{i,k|_S} \phi_{i,\ell|_S} \, \mathrm{d}\gamma,$$

9

$k, \ell = 1, \ldots, N_i$. For each fracture $F_i$, we set $N_{\mathcal{S}_i}^i = \sum_{S_m \in \mathcal{S}_i} N_m^\star$ as the number of DOFs on traces of $F_i$ on the $F_i$ "side", and we define matrices $\mathcal{B}_i \in \mathbb{R}^{N_i \times N_{\mathcal{S}_i}^i}$ grouping row-wise matrices $B_{i,m}^\star$, with $m$ spanning traces in $\mathcal{S}_i$, and setting for each $m$ either $\star = +$ or $\star = -$ according to which one of the two "sides" of trace $S_m$ is on $F_i$. Matrices $\mathcal{B}_i$ act on a column vector $u_i'$ containing all the $N_{\mathcal{S}_i}^i$ control DOFs corresponding to the traces of $F_i$, obtained extracting from $u$ blocks $u_m^\star$, for $S_m \in \mathcal{S}_i$, and appending them in the same order used in the definition of $\mathcal{B}_i$. Again, this can be obtained as the action of a suitable operator $\tilde{R}_i : \mathbb{R}^{N^T} \mapsto \mathbb{R}^{N_{\mathcal{S}_i}^i}$ such that $u_i' = \tilde{R}_i u$. In practice, $\tilde{R}_i$ extracts from $u$ only sub-vectors $u_m^\star$ corresponding to control functions on the "correct side" of the trace.

The algebraic formulation of the primal equations (7) is then

$$A_i h_i = \tilde{q}_i + \mathcal{B}_i u_i', \qquad i = 1, \ldots, I, \tag{11}$$

where $\tilde{q}_i$ accounts for the term $q_i$ in (7) and for the Neumann boundary conditions on the fracture $F_i$.

We set $A = \operatorname{diag}(A_i, i = 1, \ldots, I) \in \mathbb{R}^{N^F \times N^F}$ and define $\mathcal{B} \in \mathbb{R}^{N^F \times N^T}$ as

$$\mathcal{B} = \begin{pmatrix} \mathcal{B}_1 R_1' \\ \vdots \\ \mathcal{B}_I R_I' \end{pmatrix}.$$

Setting $q = (\tilde{q}_1, \ldots, \tilde{q}_I) \in \mathbb{R}^{N^F}$, constraints (11) are then written $Ah - \mathcal{B}u = q$.

The problem under consideration is therefore reformulated as the following equality constrained quadratic programming problem:

$$
\begin{aligned}
\min \ J(h, u) \ &= \ \frac{1}{2} \left( h^T (G^h + D) h - \alpha h^T B u - \alpha u^T B^T h \right) \\
&\quad + \frac{1}{2} \left( u^T G^u u \right) - \left( h^T h_D + h^T D^u u \right) + c \\
\text{s.t.} \quad & Ah - \mathcal{B}u = q.
\end{aligned}
$$

By (formally) exploiting the constraints $Ah = \mathcal{B}u + q$ for eliminating $h$ from the functional, we obtain the unconstrained minimization problem $\min \hat{J}(u)$, with

$$
\begin{aligned}
\hat{J}(u) = \frac{1}{2} u^T \Big( &\mathcal{B}^T A^{-T} (G^h + D) A^{-1} \mathcal{B} + G^u \tag{12} \\
&- \alpha \mathcal{B}^T A^{-T} B - \alpha B^T A^{-1} \mathcal{B} - 2 \mathcal{B}^T A^{-T} D^u \Big) u + \\
&q^T A^{-T} \left( (G^h + D) A^{-1} \mathcal{B} - \alpha B - D^u \right) u - h_D^T A^{-1} \mathcal{B} u \\
=: \ &\frac{1}{2} u^T \hat{G} u + \hat{q}^T u
\end{aligned}
$$

The unconstrained minimization problem can be solved without explicitly assembling the matrix $\hat{G}$, but rather applying an iterative solver in a *quasi*-matrix-free manner to the minimization of $\hat{J}(u)$. By applying, e.g., a gradient based method such as the Preconditioned Conjugate Gradient (PCG) method, the repeated computation of the gradient of $\hat{J}$ essentially calls for the solution of linear systems involving the (block-diagonal) matrix $A$ at each iteration, and this in turn corresponds to solving *local* linear systems with matrices $A_i$, for $i = 1, \ldots, I$. These computations can be performed in parallel. For details, we refer the reader to [18].

## 4. Numerical issues

This Section is devoted to the description of some numerical issues to be addressed for effective DFN simulations with the proposed optimization approach. We first deal with issues related to the use of the XFEM, concerning the possibility of generating linearly dependent, or nearly linearly dependent basis functions in the discrete functional space of the method. Despite effective solution to this problem are available in some circumstances (see [22]) the complexity of DFN simulations requires a customized approach. Next, we tackle the resolution of DFN problems with very small fracture transmissivity values, which usually result in very small fluxes through the network, which might negatively affect the convergence of the optimization approach.

### 4.1. Ill conditioning prevention

According to the approach depicted in Section 2, matching conditions along traces are not exactly imposed but they are made as small as possible via the optimization approach. Within the process for the minimization of $\hat{J}(u)$, only *local* problems on fractures are independently solved. As a consequence, meshes on the fractures are neither required to conform to each other, nor to conform to the traces. Clearly, the finer is the grid, the smaller is the global mismatch provided by $J$. Since the solution may present a non-smooth behavior across the traces, a possible approach for providing a better description of the solution in the case of non-conforming meshes is given by the use of XFEM. The XFEM can reproduce irregular solutions by means of custom enrichment functions that are added to the trial and test functional spaces of standard finite elements, in order to provide the discrete solution with the required non-smooth behavior, independently of the position of mesh elements with respect to the interfaces. Nevertheless, the XFEM stiffness matrix $A$ might result ill conditioned or even singular due to the presence of almost linearly or linearly dependent basis functions in the enriched functional space. When two (or more) parallel traces are present in

11

the same mesh element, the local enrichment functions are generated starting from global functions that differ only for a translation. This translation, besides being necessary in order to reproduce the behaviour of the solution, is also enough to provide linear independence of enrichment functions in the mesh element under consideration. On the other hand, linear dependencies in the local enrichment functions of neighbouring elements can arise. Almost parallel traces may also result in a ill-conditioned stiffness matrix, or even numerically singular. Preventive detection of redundant basis functions, which is a typical choice in some cases [22], is infeasible in this context due to the complex geometrical configuration of realistic DFNs. For this reason, we adopt here a different approach which consists in detecting (almost) linearly dependent rows and columns in $A$ after having assembled the matrix on each fracture. This is done operating a rank revealing QR-factorization of $A$ (see for example [23]), exploiting the special structure of the stiffness matrix. Indeed, since the matrix $A$ is a block diagonal matrix, being the $A_i$ block given by the stiffness matrix built on fracture $F_i$, the $QR$ factorization is actually independently computed for each diagonal block; since on each fracture we have a moderate amount of DOFs, the cost for computing the $QR$ factorizations is easily affordable. Furthermore, this procedure is only performed for fractures with nearly parallel traces with mutual distance smaller than the maximum element diameter. This precaution further reduces the computational cost, as the detection of parallel traces and computation of their distance is a cheap task.

After having computed the rank revealing $QR$ factorization for each diagonal block, i.e. $A_i = Q_i R_i$, with diagonal entries of the upper triangular matrix $R_i$ sorted in descending order with respect to their absolute value, we neglect rows and columns corresponding to diagonal entries whose size is smaller than a prescribed drop tolerance $\sigma$. Note that factors $Q_i$ and $R_i$ can then be used for solving the local linear system involving matrix $A_i$.

*4.2. Tackling small transmissivities*

We consider here the quite realistic case in which the network presents fracture transmissivities spanning a wide range of values (i.e., several orders of magnitude) and having *small* values, in the sense that the flux term of the functional becomes orders of magnitude smaller than the hydraulic head term. This situation is detrimental for the convergence of the method. Indeed, in these cases the contribution of the flux in the cost functional is less relevant than the hydraulic head contribution, and many iterations are required before the hydraulic head term is reduced to the same order of magnitude of the flux term. Furthermore, the flux part $\left[\!\!\left[ \frac{\partial H_i}{\partial \hat{\nu}^i_{S_m}} \right]\!\!\right]_{S_m}$ becomes

12

negligible with respect to the term $H_{i|S_m}$ in the control variable $U_i^m$ (see Eq. (4)), which also has a negative impact on the behaviour of the method. In these situations it is beneficial to resort to the resolution of a modified problem, featuring the same solution in terms of hydraulic head, but with rescaled fluxes. In order to show how the modified problem is defined, let us compactly write the original problem on a DFN $\Omega$ as follows:

$$(\mathrm{P}_a) \quad \begin{cases} -\mathrm{div}(\mathbf{K}_a \nabla h_a) & = q_a & \text{in } \Omega \setminus \mathcal{S} \\ h_a & = G^D & \text{on } \Gamma^D \\ \mathbf{K}_a \dfrac{\partial h_a}{\partial n} & = G_a^N & \text{on } \Gamma^N \end{cases}$$

completed by the additional matching conditions on the traces. In $(\mathrm{P}_a)$, $q_a$ is a source term, $G^D$ and $G_a^N$ are the functions prescribing the Dirichlet and Neumann boundary conditions respectively, and $n$ is the outward unit normal vector to $\Gamma^N$. We introduce now the modified problem $(\mathrm{P}_b)$ in such a way that, as far as the hydraulic head is concerned, $(\mathrm{P}_b)$ has the same solution $h_a$ as $(\mathrm{P}_a)$, but the fluxes are different, due to a different fracture transmissivity value. The modified problem is defined as:

$$(\mathrm{P}_b) \quad \begin{cases} -\mathrm{div}(\mathbf{K}_b \nabla h_a) & = q_b & \text{in } \Omega \setminus \mathcal{S} \\ h_a & = G^D & \text{on } \Gamma^D \\ \mathbf{K}_b \dfrac{\partial h_a}{\partial n} & = G_b^N & \text{on } \Gamma^N \end{cases}$$

with additional matching conditions on the traces, and with $\mathbf{K}_b = k\mathbf{K}_a$, $q_b = kq_a$, $G_b^N = kG_a^N$, being $k$ a given scalar value. It is straightforward to prove that, with such rescaling, all the fluxes in $(\mathrm{P}_b)$ are rescaled by a factor $k$ with respect to the fluxes obtained for $(\mathrm{P}_a)$. Choosing $k \gg 1$, the fluxes for problem $(\mathrm{P}_b)$ will be larger than the fluxes for $(\mathrm{P}_a)$, thus improving the numerical behavior of the optimization algorithm. We remark that this approach is more effective than the mere application of the penalty factor to the flux term in the functional, as with this choice it is possible to control the weight of the flux terms w.r.t. the hydraulic head terms both in the cost functional and in the control variables. Our numerical experience has shown that, with a scalar transmissivity, in most situations the choice $k = 1/\min(K_a)$ gives good results. In the general case, one can relate the parameter $k$ to the minimum among all eigenvalues of the transmissivity tensors.

## 5. Numerical results

In this section we discuss some numerical results in order to describe the capabilities of the improved method here presented. We start with some
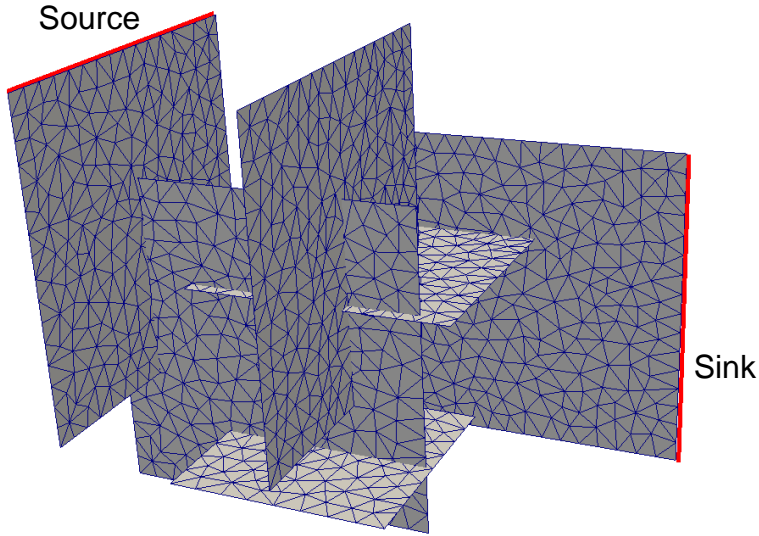
Figure 1: DFN configuration for TP1a and TP1b with illustrative mesh. Boundaries with Dirichlet conditions marked with thicker line

investigations on rather simple DFN configurations in order to assess the behavior of the method on benchmark problems. Next, we report on simulations on more realistic networks.

All the simulations are performed using first order finite elements with the XFEM on non-conforming meshes. The computational mesh is built on each fracture of the considered DFNs independently, regardless of the position of the intersections with the other fractures. The mesh size is related to the mesh parameter $\delta$, representing the maximal element area. As mentioned, standard FEM or the VEM could be used as an alternative for the discretization of the variables, see [16, 17].

As a preconditioner for the PCG method applied to functional (12) (i.e., to matrix $\hat{G}$), we used the block diagonal matrix $P$ formed by the mass matrices $C_m^-$ and $C_m^+$, $m \in \mathcal{M}^{\text{int}}$, and $C_m^D$, $m \in \mathcal{M}^{\text{D}}$.

In the rank revealing $QR$ factorization for $A_i$, $i = 1, ..., I$, the drop tolerance $\sigma$ has been set to $10^{-9} \max_k |(R_i)_{k,k}|$.
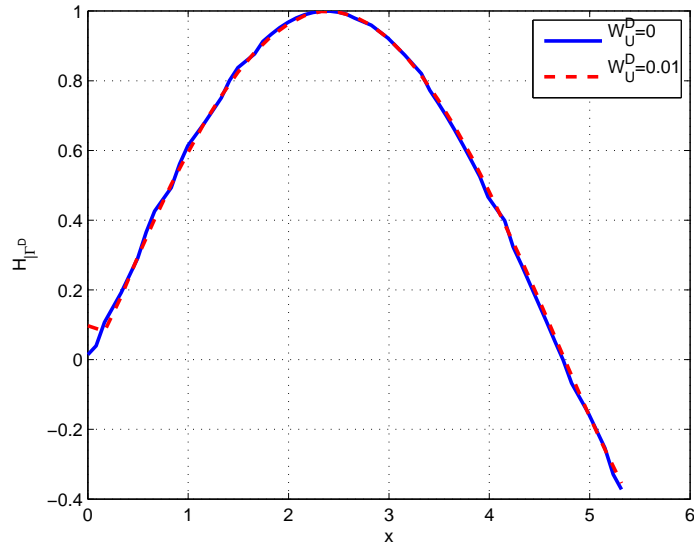
Figure 2: Reproduced boundary condition for test problem TP1a on the finer mesh and two values of parameter $\mathcal{W}_U^D$
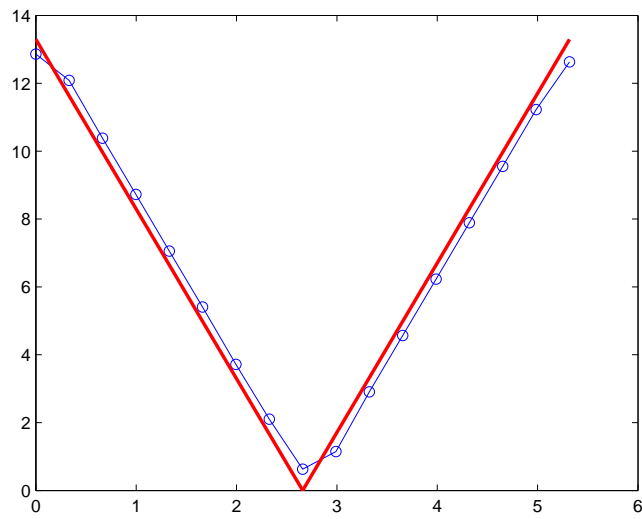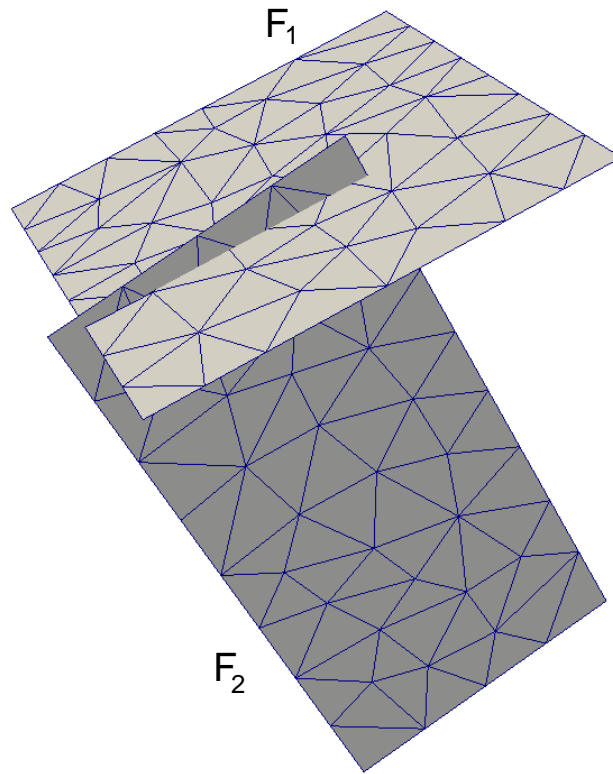


Figure 3: Reproduced boundary condition compared with exact value for test problem TP1b

15

Table 1: TP1a: Relative difference in L$^2$ norm between the computed solution and the exact boundary condition on the source fracture

| $\delta$ | $\mathcal{W}_U^D$ | $\mathcal{W}_H^D$ | $\|H_{|\Gamma^D} - G^D\|/\|G^D\|$ |
|------|------|------|------------------------|
| 0.1 | 0 | 1 | 4.861e-3 |
| 0.1 | 0.01 | 1 | 1.088e-2 |
| 0.01 | 0 | 1 | 5.246e-4 |
| 0.01 | 0.01 | 1 | 1.176e-3 |
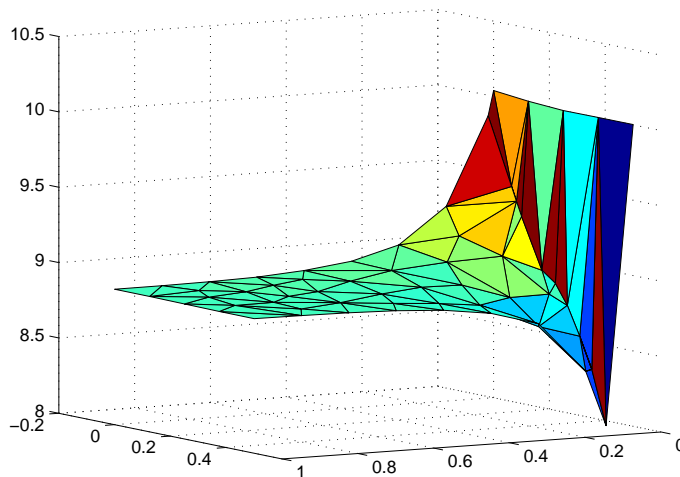
Figure 4: TP1c: DFN with the computational mesh (left) and solution (right) on fracture $F_2$

### 5.1. The boundary conditions

The first set of examples deals with the imposition of boundary conditions in weak form as described in Section 2. Three different test problems are proposed, labeled TP1a, TP1b and TP1c. Problems TP1a and TP1b share the same fracture network geometry, shown in Figure 1 along with an example of nonconforming computing mesh, but with different boundary condition settings. The DFN is made of six fractures with areas ranging from $12\text{m}^2$ to $28\text{m}^2$; with reference to Figure 1, the fracture labeled as *source* carries a non-homogeneous Dirichlet boundary condition on the edge marked with a thicker line, while the *sink* fracture has a homogeneous Dirichlet boundary condition on the marked edge. All other fracture edges are insulated, i.e. homogeneous Neumann boundary conditions are set. For test TP1a the Dirichlet boundary condition on the source fracture is a smooth sinusoidal function, and two different meshes have been considered, corresponding to mesh parameters $\delta = 0.1$ and $\delta = 0.01$. Results for test TP1a are reported in Table 1 for the two grids and two choices of the parameter $\mathcal{W}_U^D$, while $\mathcal{W}_H^D$ is set to one for all the simulations. Namely, the table reports the relative errors between the solution computed at the boundary and the Dirichlet data $G^D$. As expected, for fixed values of the parameter $\mathcal{W}_U^D$, the approximation improves as the mesh is refined, whereas it is possible to notice that, on a fixed grid the value $\mathcal{W}_U^D = 0$ provides a better result than $\mathcal{W}_U^D = 0.01$. However, looking at Figure 2, which represents the solution computed on the

Table 2: Value of the hydraulic head on selected traces for $TP2a$ and $TP2b$ compared with the analytical solution

| Trace number | Exact solution | $\Delta\ TP2a\ modified$ | $\Delta\ TP2b\ modified$ |
|:---:|:---:|:---:|:---:|
| 1 | 9.842346 | 3.57e-8 | 3.0e-6 |
| 5 | 9.839824 | 5.15e-8 | 1.35e-3 |
| 10 | 9.839388 | 5.5e-8 | 4.46e-4 |
| 15 | 2.185697 | 2.24e-7 | 2.1e-4 |
| 20 | 1.405312 | 1.72e-7 | 1.08e-4 |
| 25 | 1.141987 | 1.35e-7 | 1.37e-5 |
| 29 | 1.000574 | 4.32e-9 | 2.09e-6 |

Dirichlet boundary with the finest mesh and with the two values of $\mathcal{W}_U^D$, it appears that the choice $\mathcal{W}_U^D = 0.01$ provides a smoother approximation. Numerical experiments showed that further increasing the value of $\mathcal{W}_U^D$ rapidly deteriorates the quality of the reproduced boundary condition.

The boundary condition for TP1b on the source fracture is a non-smooth function presenting a kink. Also in this case, the obtained value is compared to the exact solution in Figure 3. The irregular behavior is correctly reproduced.

The geometry for TP1c is reproduced in Figure 5.1. With reference to this figure, a constant non-homogenous Dirichlet boundary condition ($h = 10$) is prescribed on the top edge of fracture $F_2$, and an homogeneous Dirichlet boundary condition is set on the right edge of fracture $F_1$. All other edges are insulated. The peculiarity of this test problem is that the intersection between the two fractures lies very close to the Dirichlet boundary of fracture $F_2$. In these circumstances the imposition of Dirichlet boundary conditions on $F_2$ is complex, requiring the resolution of additional local problems, in order to correctly reproduce both the boundary condition and the irregular behaviour of the solution across the traces. The weak imposition of boundary conditions by means of the cost functional allows to overcome these complexities in a straightforward manner. The solution obtained on $F_2$ is reported in Figure 4, showing that the boundary condition is correctly reproduced. At the same time the jump of solution gradient across the trace is correctly catch.

*5.2. Tackling small transmissivities*

The next two test problems, labeled TP2a and TP2b, respectively, aim at showing the effectiveness of the approach proposed in Subsection 4.2, intended to improve the numerical results when the transmissivities in the network are very small and span several orders of magnitude. The geometry
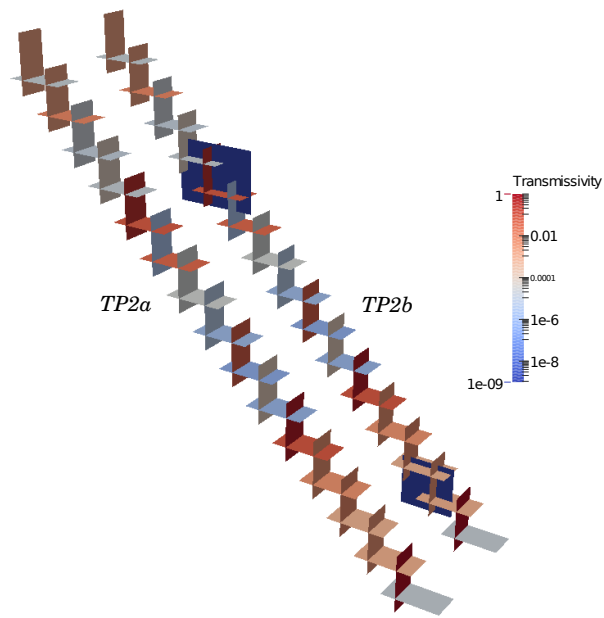
Figure 5: DFN configuration for TP2a and TP2b with distribution of fracture transmissivity

is depicted in Figure 5: problem TP2b is obtained adding two fractures to the geometry of TP2a. Traces are numbered from top to bottom for the geometry used for TP2a, with a total of 29 traces, and the same numbering is maintained for the corresponding traces of TP2b, with the additional traces numbered consecutively. For these simulations the transmissivity $K_i$ is constant on each fracture $F_i$; its distribution among the fractures is reported in Figure 5 through the colorbar. On the two additional fractures introduced in TP2b the transmissivity is set to the value $K = 10^{-9}$, i.e., two orders of magnitude lower than the minimum value used for TP2a. The same boundary conditions are prescribed for the two problems: a constant hydraulic head ($h = 10$) is set on the top edge of the top fracture, whereas a homogeneous Dirichlet condition is set on the bottom edge of the bottom fracture. The wide range of transmissivities considered ($K_i \in [10^{-7}, 1]$ for TP2a and $K_i \in [10^{-9}, 1]$ for TP2b) makes the problems very challenging, in particular due to the presence of values of $K \ll 1$. Due to the special structure of problem TP2a, the analytical solution can be computed for this problem, and it has been used to assess the accuracy of the obtained solution. Furthermore, since TP2b is obtained from TP2a by adding two fractures with a very low transmissivity, the solution of TP2b is a small perturbation of the solution of TP2a. As a consequence, we compared also the numerical results obtained for TP2b with the analytical solution for TP2a, showing that the proposed numerical approach correctly accounts for the marginal effect of the added fractures.

We remark that when approaching the problem in its original formulation, it is quite hard to obtain an accurate solution, due to the fact that the fluxes are too small compared to the values of the hydraulic head, and consequently numerical approximation errors affect the definition of the control variables, and the flux-related term contributes to a very small extent to the minimization process. In Table 2 we report some results obtained for TP2a and TP2b with the modified problem ($P_b$). Namely, the second column reports the analytical solution of the hydraulic head for TP2a on selected traces; the third column shows the errors in the numerical solution; the fourth column reports the distance of the numerical solution obtained for TP2b from the exact solution of TP2a.

### 5.3. Realistic DFNs

We now turn our attention to more realistic DFN configurations. First, we consider a network composed of 68 fractures and 142 traces (labeled DFN68), with fracture areas spanning from $2.83 \times 10^3 \mathrm{m}^2$ to $1.13 \times 10^4 \mathrm{m}^2$; the network is shown in Figure 6. Also in this case the flow occurs between a source fracture with a constant Dirichlet boundary condition $h = 100$ on one edge and a
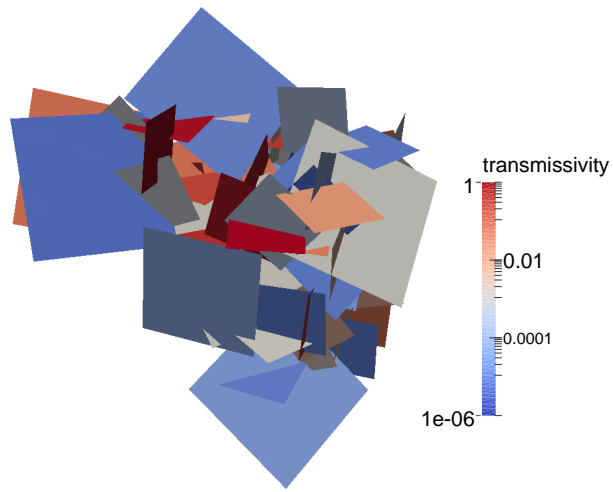
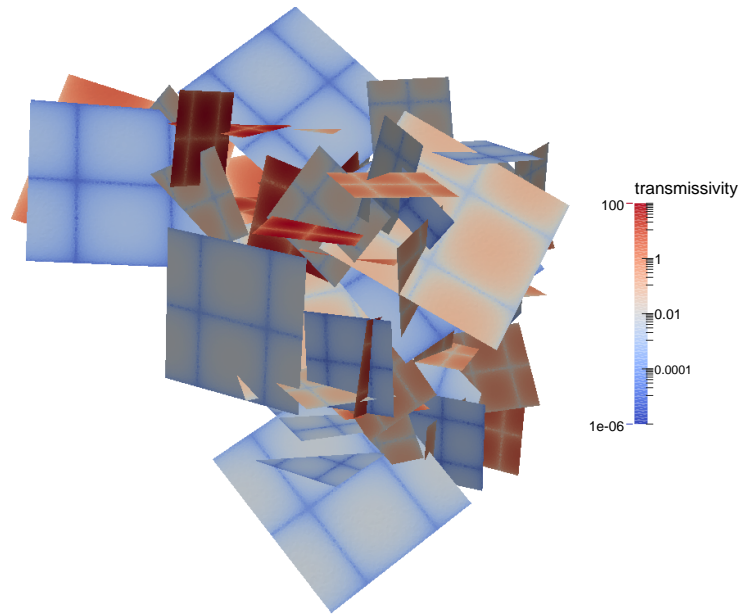Figure 6: DFN68: fracture transmissivity distribution for configuration I



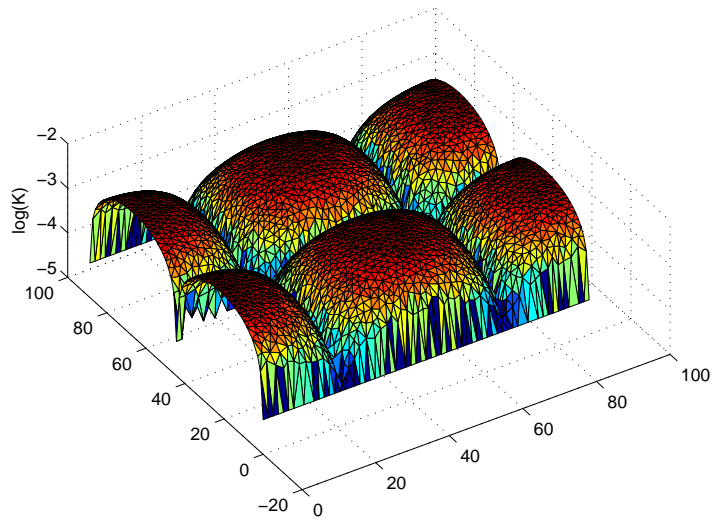Figure 7: DFN68: fracture transmissivity distribution for configuration II

21

Figure 8: DFN68: fracture transmissivity on the source fracture, configuration II
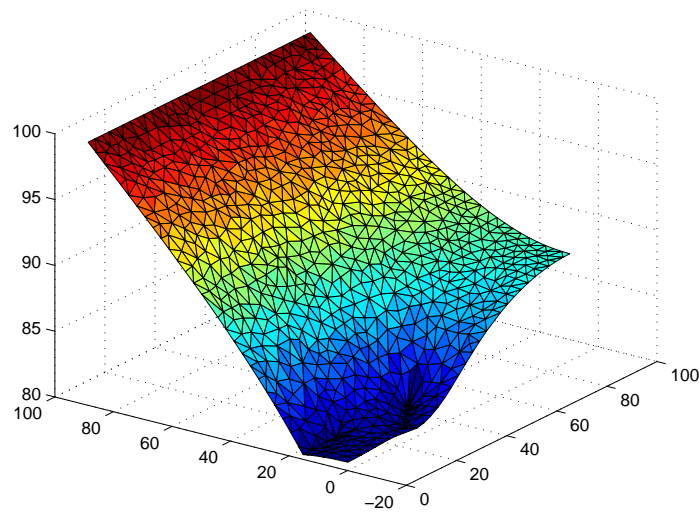


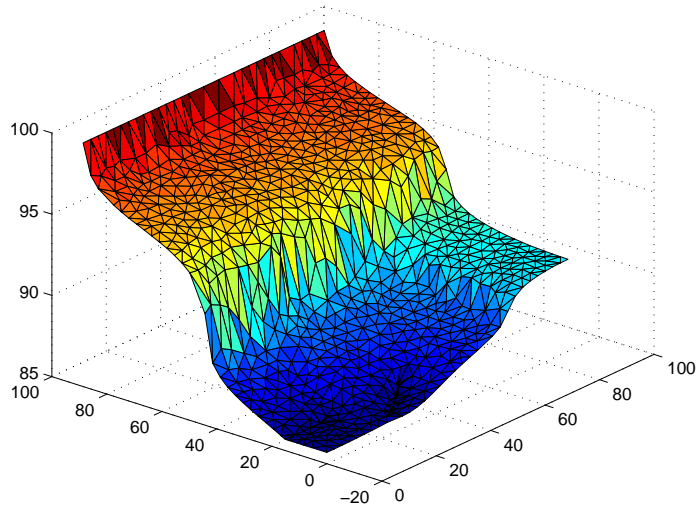Figure 9: DFN68: hydraulic head on the source fracture for configuration I; $\delta = 8$.

22

Figure 10: DFN68: hydraulic head on the source fracture for configuration II; $\delta = 8$.

Table 3: DFN68, configurations I: error indicators

| $\mathcal{W}_U$ | $\Delta_{\text{head}}$ | $\Delta_{\text{flux}}$ | $\Delta_{\text{cons}}$ |
|---|---|---|---|
| $\delta = 128$ | | | |
| 1 | 1.569e-5 | 1.585e-6 | 1.463e-1 |
| 10 | 2.085e-5 | 1.449e-6 | 2.835e-2 |
| 100 | 4.473e-5 | 8.441e-7 | 5.209e-3 |
| 500 | 6.668e-5 | 4.450e-7 | 8.235e-4 |
| $\delta = 32$ | | | |
| 1 | 8.863e-6 | 6.219e-7 | 2.348e-2 |
| 10 | 1.015e-5 | 3.065e-7 | 3.247e-3 |
| 100 | 1.386e-5 | 1.657e-7 | 2.508e-4 |
| 500 | 1.837e-5 | 8.291e-8 | 3.450e-4 |
| $\delta = 8$ | | | |
| 1 | 6.216e-6 | 5.399e-7 | 1.915e-2 |
| 10 | 7.905e-6 | 2.132e-7 | 2.795e-3 |
| 100 | 9.749e-6 | 9.437e-8 | 2.199e-4 |
| 500 | 1.147e-5 | 6.679e-8 | 4.553e-5 |
| $\delta = 2$ | | | |
| 1 | 2.309e-6 | 2.945e-7 | 8.157e-4 |
| 10 | 3.451e-6 | 1.343e-7 | 2.508e-5 |
| 100 | 5.093e-6 | 7.209e-8 | 5.620e-5 |
| 500 | 7.386e-6 | 3.866e-8 | 2.048e-5 |

23

Table 4: DFN68, configuration II: error indicators

| $\mathcal{W}_U$ | $\Delta_{\text{head}}$ | $\Delta_{\text{flux}}$ | $\Delta_{\text{cons}}$ |
|---|---|---|---|
| | $\delta = 8$ | | |
| 1 | 2.787e-5 | 8.247e-8 | 8.148e-4 |
| 10 | 3.254e-5 | 2.633e-8 | 1.097e-4 |
| 100 | 3.621e-5 | 9.142e-9 | 1.504e-5 |
| 500 | 3.929e-5 | 5.666e-9 | 5.644e-6 |
| | $\delta = 2$ | | |
| 1 | 7.680e-6 | 6.043e-8 | 8.849e-5 |
| 10 | 1.375e-5 | 2.679e-8 | 2.742e-5 |
| 100 | 2.095e-5 | 1.260e-8 | 7.160e-6 |
| 500 | 2.888e-5 | 6.521e-9 | 3.516e-6 |

sink fracture with an homogeneous Dirichlet boundary condition, all other fracture edges being insulated. The same geometry is accompanied by two different hydraulic transmissivity configurations: configuration I, in which a constant value transmissivity is set on each fracture, and configuration II in which the hydraulic transmissivity displays strong variations on each fracture. The distribution of the hydraulic transmissivity for this problem is shown in Figures 6-7 for the two configurations. More in detail, the values of the transmissivity on the source fracture are plotted in Figure 8; this behaviour is representative for all the fractures. We have considered four different mesh parameters, ranging from $\delta = 128$ (corresponding to 6759 total degrees of freedom) to $\delta = 2$ (resulting in 144738 total degrees of freedom). For configuration II we used only the two finest meshes, in order to be able to resolve the variability of the coefficients. In all the simulations reported we used the modified problem $(P_{\text{b}})$. The solutions obtained on the source fracture, with both configurations, and using the mesh parameter $\delta = 8$, are reported in Figures 9-10.

The quality of the solution is evaluated in terms of the following error measures on the internal traces, as the error on the Dirichlet traces is nearly the round-off error due to the fact that the Dirichlet data are constant. We define the relative mismatch in hydraulic head continuity per trace length as

$$\Delta_{\text{head}} = \frac{\sqrt{\sum_{m\in\mathcal{M}^{\text{int}}} \left\| h_{i|_{S_m}} - h_{j|_{S_m}} \right\|^2}}{h_{\max}L},$$

being $L = \sum_{m\in\mathcal{M}^{\text{int}}} |S_m|$ the cumulative trace length. Furthermore, let $\mathcal{I}_{\text{in}}$ and $\mathcal{I}_{\text{out}}$ denote the index sets corresponding to source and sink fractures, re-

24

Table 5: DFN909: number of iterations performed and error measures

| | Iterations | | Error measures | | |
|---|---|---|---|---|---|
| $\delta$ | non prec | prec | $\Delta_{\text{head}}$ | $\Delta_{\text{flux}}$ | $\Delta_{\text{cons}}$ |
| 7 | 124038 | 27779 | 1.324e-6 | 5.650e-10 | 4.326e-5 |
| 2 | 87902 | 24895 | 8.937e-7 | 3.825e-10 | 3.717e-5 |
| 0.5 | 42792 | 25259 | 5.213e-7 | 2.384e-10 | 4.895e-5 |

spectively, and let $\bar{\bar{\Phi}}$ denote the computed average flux through the network, i.e.,

$$
\bar{\bar{\Phi}} = \frac{1}{2} \left( \sum_{i \in \mathcal{I}_{\text{in}}} \sum_{S_m \in \mathcal{S}_i^{\text{int}}} \int_{S_m} (u_i^m - \alpha_m h_{i|S_m}) \right.
$$

$$
\left. - \sum_{i \in \mathcal{I}_{\text{out}}} \sum_{S_m \in \mathcal{S}_i^{\text{int}}} \int_{S_m} (u_i^m - \alpha_m h_{i|S_m}) \right).
$$

The relative flux unbalance per trace length is defined as

$$
\Delta_{\text{flux}} = \frac{\sqrt{\sum_{m \in \mathcal{M}^{\text{int}}} \left\| u_i^m + u_j^m - \alpha_m \left( h_{i|S_m} + h_{j|S_m} \right) \right\|^2}}{\bar{\bar{\Phi}} L},
$$

and the relative conservation error per trace length as

$$
\Delta_{\text{cons}} = \frac{\left| \sum_{i \in \mathcal{I}_{\text{in}} \cup \mathcal{I}_{\text{out}}} \sum_{S_m \in \mathcal{S}_i^{\text{int}}} \int_{S_m} (u_i^m - \alpha_m h_{i|S_m}) \right|}{\bar{\bar{\Phi}}}.
$$

The computed errors are reported in Tables 3 and 4 for configuration I and II, respectively, for all mesh parameters considered in each case and for several values of the flux penalty factor $\mathcal{W}_U$, ranging from 1 to 500.

It can be noted that the use of penalty factors can be beneficial in improving the quality of the solution in terms of flux conservation and flux balance, at the expenses of a slight deterioration of the hydraulic head continuity across the traces. It appears that here higher values of $\mathcal{W}_U$ are more effective for the coarsest grid than for the finest grid, even if, however, the differences are almost negligible.

We end this section with some results concerning a DFN made of 909 fractures, with area ranging from 376m$^2$ to 10$^4$m$^2$, and 7084 traces (problem DFN909). This DFN is particularly challenging due to the presence, in the same fracture, of non intersecting traces very close to each other, and of
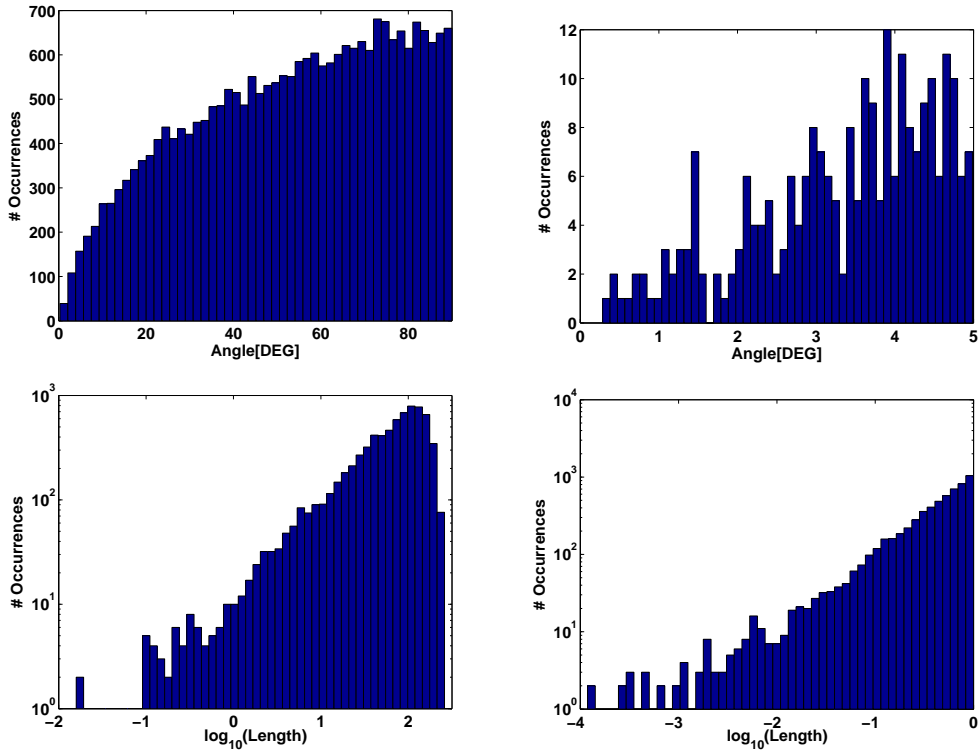
25

Figure 11: DFN909. Top: distribution of angles between pairs of intersecting traces in the same fracture; right: a detail of smallest values. Bottom: distribution of the length of traces (left) and of distances between pairs of non-intersecting traces (right).
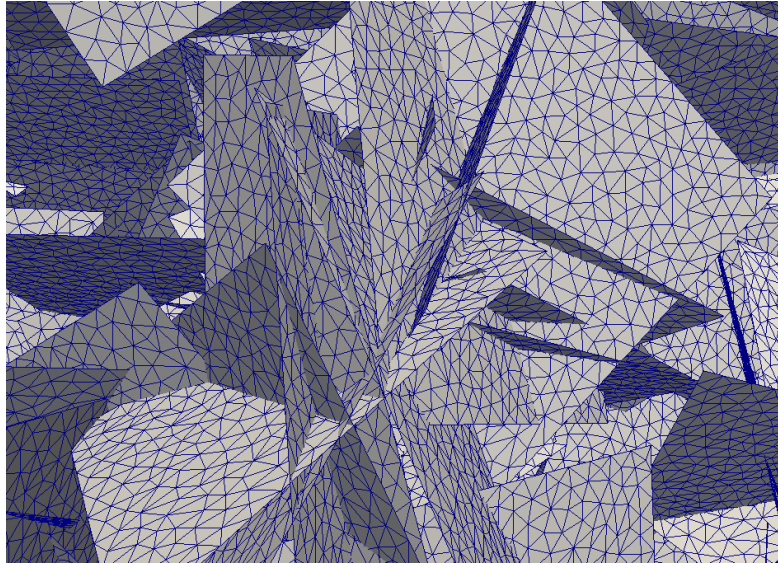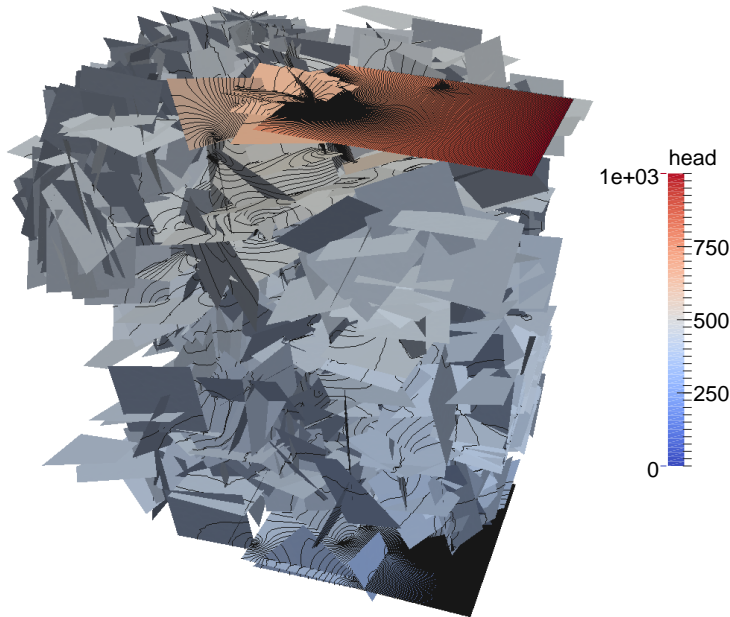


Figure 12: DFN909: detail of the finer mesh

Figure 13: DFN909: distribution of the hydraulic head. Solution on the finer mesh

traces intersecting in the same fracture with angles smaller than $1°$. These challenging geometrical features of the DFN are summarized in Figure 11, representing the distribution of angles between intersecting traces (with a zoom of the smallest values), the distribution of trace lengths in the DFN and of the distances between non intersecting traces on the same fracture.

Methods relying on some kind of mesh conformity are likely to generate on this network poor quality meshes. On the other hand, with the approach here adopted the problem can be tackled without any modification of the geometry of the DFN or any special care in the generation of a good quality mesh. Three mesh sizes have been considered: the finest mesh, corresponding to $\delta = 0.5$, yields 619,120 total degrees of freedom for the control variables and 3,132,723 degrees of freedom for the hydraulic head; the coarsest mesh corresponding to $\delta = 7$ yields 161,089 DOFs for the control variables and 572,334 DOFs for the hydraulic head. Figure 12 reports the computational mesh corresponding to $\delta = 2$, having 306,517 and 1,191,483 DOFs for the control variables and for the hydraulic head, respectively. On each fracture we set a constant fracture transmissivity, with values ranging from $10^{-4}$ to 1. Also in this case the modified problem $(P_b)$ has been considered to tackle small transmissivity values.

Numerical computations were performed on a parallel computer with 20 cores; iterations were stopped when a relative residual smaller than $10^{-6}$ was

27

met. The solution obtained on the finest mesh is reported in Figure 13, in which the colouring is proportional to the hydraulic head $h$, and iso-$h$ lines are also shown to highlight gradients.

In Table 5 we report the error measures computed on DFN909, along with the number of iterations needed to reach a relative residual smaller than $10^{-6}$. Also in this quite challenging problem, the error measures are remarkably satisfactory. In order to show the effectiveness of the preconditioner adopted, the number of iterations is compared with those needed for reaching the same accuracy without preconditioner, showing that the number of iterations is at least halved. The number of iterations also appears to be almost independent of the mesh parameter $\delta$.

Comparing the error measures of test problems DFN68 and DFN909, it is possible to see that the errors achieved are nearly of the same order of magnitude, despite the challenging geometrical features present in DFN909 and not in DFN68 (i.e., narrow angles, close traces, multi-scale distribution of fracture areas). This highlights the robustness of the method in handling such complex geometries.

## 6. Conclusions

Focusing on the resolution of the steady-state flow in large fracture networks, we have proposed further improvements with respect to previous works proposed by the authors [14, 15, 16]. Namely, a new formulation of the objective functional has been proposed, tackling the imposition of the Dirichlet boundary conditions in a weak form and thus improving the method towards an increased flexibility.

As far as the XFEM discretization is concerned, we address ill-conditioning issues; we also suggest resolution strategies in order to deal with networks of fractures characterized by a strong variability in fracture transmissivities, and/or where some fractures have an hydraulic transmissivity many orders of magnitudes smaller than the others.

A preconditioner for the resolution of discrete linear system of equations is proposed. The structure of this preconditioner is simple and effective, and it can be easily used for the resolution of the problem within a parallel approach.

All the previous issues are crucial for handling complex, large scale, heterogeneous networks without any need of *ad hoc* intervention tailored on the specific DFN.

**References**

[1] M. C. Cacas, E. Ledoux, G. de Marsily, B. Tillie, A. Barbreau, E. Durand, B. Feuga, P. Peaudecerf, Modeling fracture flow with a stochastic discrete fracture network: calibration and validation: 1. the flow model, Water Resour. Res. 26 (1990) 479–489. doi:http://dx.doi.org/10.1029/WR026i003p00479.

[2] A. W. Nordqvist, Y. W. Tsang, C. F. Tsang, B. Dverstop, J. Andersson, A variable aperture fracture network model for flow and transport in fractured rocks, Water Resource Res. 28 (1992) 1703–1713. doi:http://dx.doi.org/10.1029/92WR00216.

[3] W. S. Dershowitz, C. Fidelibus, Derivation of equivalent pipe networks analogues for three-dimensional discrete fracture networks by the boundary element method, Water Resource Res. 35 (1999) 2685–2691. doi:http://dx.doi.org/10.1029/1999WR900118.

[4] J. R. D. Dreuzy, P. Davy, O. Bour, Hydraulic properties of two-dimensional random fracture networks following a power law length distribution: 2., permeability of networks based on log-normal distribution of apertures, Water Resour. Res. 37 (8) (2001) 2079–2095. doi:http://dx.doi.org/10.1029/2001WR900010.

[5] D. Blessent, R. Therrien, C. W. Gable, Large-scale numerical simulation of groundwater flow and solute transport in discretely-fractured crystalline bedrock, Advances in Water Resources 34 (12) (2011) 1539 – 1552. doi:http://dx.doi.org/10.1016/j.advwatres.2011.09.008.

[6] B. Nœtinger, N. Jarrige, A quasi steady state method for solving transient Darcy flow in complex 3D fractured networks, J. Comput. Phys. 231 (1) (2012) 23–38. doi:http://dx.doi.org/10.1016/j.jcp.2011.08.015.

[7] G. Pichot, J. Erhel, J. de Dreuzy, A mixed hybrid mortar method for solving flow in discrete fracture networks, Applicable Analysis 89 (2010) 1629 – 643. doi:http://dx.doi.org/10.1080/00036811.2010.495333.

[8] C. Dorn, N. Linde, T. L. Borgne, O. Bour, J.-R. de Dreuzy, Conditioning of stochastic 3-d fracture networks to hydrological and geophysical data, Advances in Water Resources 62, Part A (0) (2013) 79 – 89. doi:http://dx.doi.org/10.1016/j.advwatres.2013.10.005.

[9] B. Nœtinger, A quasi steady state method for solving transient Darcy flow in complex 3D fractured networks accounting for matrix to fracture flow, J. Comput. Phys. 283 (2015) 205–223. doi:http://dx.doi.org/10.1016/j.jcp.2014.11.038.

[10] G. Pichot, J. Erhel, J. de Dreuzy, A generalized mixed hybrid mortar method for solving flow in stochastic discrete fracture networks, SIAM Journal on scientific computing 34 (2012) B86 – B105. doi:http://dx.doi.org/10.1137/100804383.

[11] J. Hyman, C. Gable, S. Painter, N. Makedonska, Conforming delaunay triangulation of stochastically generated three dimensional discrete fracture networks: A feature rejection algorithm for meshing strategy, SIAM Journal on Scientific Computing 36 (2014) A1871–A1894. doi:http://dx.doi.org/10.1137/130942541.

[12] H. Mustapha, K. Mustapha, A new approach to simulating flow in discrete fracture networks with an optimized mesh, SIAM J. Sci. Comput. 29 (4) (2007) 1439–1459. doi:http://dx.doi.org/10.1137/060653482.

[13] A. Fumagalli, A. Scotti, A numerical method for two-phase flow in fractured porous media with non-matching grids, Advances in Water Resources 62 (2013) 454 – 464. doi:http://dx.doi.org/10.1016/j.advwatres.2013.04.001.

[14] S. Berrone, S. Pieraccini, S. Scialò, A PDE-constrained optimization formulation for discrete fracture network flows, SIAM J. Sci. Comput. 35 (2) (2013) B487–B510. doi:http://dx.doi.org/10.1137/120865884.

[15] S. Berrone, S. Pieraccini, S. Scialò, On simulations of discrete fracture network flows with an optimization-based extended finite element method, SIAM J. Sci. Comput. 35 (2) (2013) A908–A935. doi:http://dx.doi.org/10.1137/120882883.

[16] S. Berrone, S. Pieraccini, S. Scialò, An optimization approach for large scale simulations of discrete fracture network flows, J. Comput. Phys. 256 (2014) 838–853. doi:http://dx.doi.org/10.1016/j.jcp.2013.09.028.

[17] M. F. Benedetto, S. Berrone, S. Pieraccini, S. Scialò, The virtual element method for discrete fracture network simulations, Computer Methods in Applied Mechanics and Engineering 280 (0) (2014) 135 – 156. doi:http://dx.doi.org/10.1016/j.cma.2014.07.016.

[18] S. Berrone, S. Pieraccini, S. Scialò, F. Vicini, A parallel solver for large scale DFN flow simulations, SIAM J. Sci. Comput. 37 (3) (2015) C285–C306. doi:http://dx.doi.org/10.1137/140984014.

[19] S. Berrone, C. Canuto, S. Pieraccini, S. Scialò, Uncertainty quantification in discrete fracture network models: stochastic fracture transmissivity, to appear in Computers & Mathematics with Applications.

[20] T.-P. Fries, T. Belytschko, The extended/generalized finite element method: an overview of the method and its applications, Internat. J. Numer. Methods Engrg. 84 (3) (2010) 253–304. doi:http://dx.doi.org/10.1002/nme.2914.

[21] S. Osher, R. Fedkiw, Level set methods and dynamic implicit surfaces, Vol. 153 of Applied Mathematical Sciences, Springer-Verlag, New York, 2003.

[22] T.-P. Fries, A corrected xfem approximation without problems in blending elements, Internat. J. Numer. Methods Engrg. 75 (2008) 503–532. doi:http://dx.doi.org/10.1002/nme.2259.

[23] P. E. Gill, W. Murray, M. H. Wright, Numerical linear algebra and optimization, Addison-Wesley Pub. Co., 1991.